A Telescope Search for Decaying Relic Axions

astro-ph/0611502

Daniel Grin[1], Giovanni Covone[2], Jean-Paul Kneib[3], Marc Kamionkowski[1], Andrew Blain[1], Eric Jullo[4]

[1] *California Institute of Technology*, [2] *INAF*, [3] *OAMP Marseilles*, [4] *European Southern Observatory*

Abstract:

We searched for optical line emission from the two-photon decay of relic axions in the galaxy clusters Abell 2667 and 2390, using spectra from the Visible Multi-Object Spectrograph (VIMOS) Integral Field Unit (IFU) at the Very Large Telescope (VLT). New upper limits to the two-photon coupling of the axion are derived, and are at least a factor of 3 more stringent than previous upper limits in this mass window. The improvement follows from larger collecting area, integration time, and spatial resolution, as well as from improvements in signal to noise and sky subtraction made possible by strong-lensing mass models of these clusters. The new limits either require that the two-photon coupling of the axion be extremely weak or that the axion mass window between 4.5 eV and 7.7 eV be closed. We also discuss briefly implications for sterile-neutrino dark matter.

I. Axions as Dark Matter

Due to non-perturbative effects, the effective Lagrangian for QCD has a CP-violating term (this is the strong CP problem), which predicts a neutron electric dipole moment of $d_n = 10^{-16}\ \theta$ e cm; experimental constraints require that $\theta \ll 10^{-10}$, presenting a fine-tuning problem that can be solved by introducing a new complex pseudoscalar field with a new high-energy symmetry, the Peccei-Quinn scale (Peccei and Quinn, 1977). Excitations of the phase of this field are known as **axions** and have mass

$$m_{\rm a} = \frac{m_\pi f_\pi}{f_{\rm PQ}/N}\frac{\sqrt{z}}{1+z}, \qquad (1)$$

where $z \equiv m_u/m_d$. Because the PQ scale is *apriori* unconstrained, $m_{\rm a}$ could conceivably have a wide range. However, experimental searches and astrophysical constraints leave the mass windows $10^{-5} - 10^{-3}$ eV and $3 - 8$ eV (for hadronic axions) open. Axion decays/annihilations to standard model particles scale as α^2, so axions are a natural candidate for the dark matter, in this most conservative possible extension of the standard model.

Fig. 1

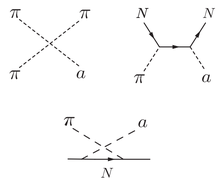

If $m_{\rm a} > 10^{-2}$ eV, axions will come into thermal equilibrium via the processes shown in Fig. 1, and freeze out near $T_d \simeq 40 - 50$ MeV to yield an abundance today of (Turner 1988, Chang and Choi 1993)

$$\Omega_a h^2 \simeq \frac{m_{\rm a}}{130\ {\rm eV}}, \qquad (2)$$

implying that $\sim$ eV axions could be a significant fraction of a warm dark matter component.

II. Axion Decay to Two Photons

In DFSZ models, axions couple to SM quarks through triangle anomaly diagrams, and then decay directly to photon pairs. In KSVZ models, axions do not directly couple to SM quarks. Through their coupling to gluons, they decay to pions (See Fig. 2). These pions then decay to photons. The DFSZ model shares this channel. The resulting axion lifetime is

$$\tau = 6.8\times10^{24}\xi^{-2}m_{\rm a,eV}^{-5}\ {\rm s}, \qquad (3)$$
$$\text{where } \xi \equiv \frac{4}{3}\left(E/N - 1.92 \pm 0.08\right).$$

In DFSZ models, $E/N = 8/3$, while in KSVZ models, $E/N = 2$. In KSVZ models, ξ may vanish (Moroi and Murayama 1998), so if telescope time is available, it pays to keep looking! The resulting line emission will be at

$$\lambda_a = \frac{24,800\text{Å}}{m_{\rm a,eV}}. \qquad (4)$$

Due to the extremely low rate, natural line broadening is negligible.

Fig. 2

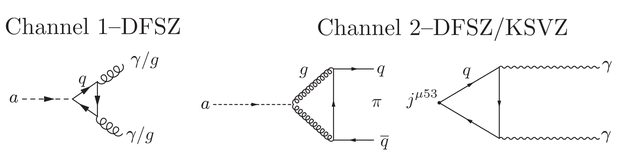

III. Axions in Galaxy Clusters

Following the evolution of axion velocities with the Boltzmann equation, today thermal axions have velocities $\langle v_{\rm a}^2/c^2\rangle^{1/2} = 4.9\times10^{-4}m_{\rm a,eV}^{-1}$ (Turner 1988), low enough that axions will bind to galaxy clusters. Assuming a King profile, the maximum axion mass fraction of a bound system is

$$x_{\rm a}^{\rm max} = 1.2\times10^{-2}m_{\rm a,eV}^4\left(\frac{a}{250\ h^{-1}{\rm kpc}}\right)^2\left(\frac{\sigma}{1000\ {\rm km\ s^{-1}}}\right), \qquad (5)$$

so unlike single galaxies, galaxy clusters have ample phase space to accomodate an axion mass fraction $x_a = \Omega_a/\Omega_m$

The expected line intensity is

$$\mathbf{I_{\lambda_o} = 2.68\times10^{-18}\times\frac{m_{a,eV}^7\xi^2\Sigma_{12}\exp\left[-(\lambda_r-\lambda_a)^2c^2/\left(2\lambda_a^2\sigma^2\right)\right]}{\sigma_{1000}(1+z_{cl})^4S^2(z_{cl})}cgs}, \qquad (6)$$

where $S^2(z_{\rm cl})$ is the dimensionless angular diameter distance to the cluster

Such a signal could feasibly be detected, but the intensity is nearly equal to that of the night-sky continuum, so care must be taken when subtracting the sky background. Fortunately, the expected line traces the projected density of the cluster, providing a natural way to implement this subtraction. Searches for this emission were first suggested by Kephart and Weiler (1987). Turner extended this suggestion to clustered axions (1988).

The first observational attempt was made by Bershady, Ressell, and Turner (1991). These workers took spectra of three clusters at KPNO, laying spectral slits down throughout the cluster, extending from the cluster core to the edge. Spectra from the outside of the cluster were subtracted from spectra taken at the cluster core; a King profile was used to translate flux limits into limits on the two photon coupling of the axion. With greater exposure, lensing derived mass maps, and spatially resolved (VIMOS IFU) spectroscopy, we conducted a more sensitive search.

IV. Data/Analysis

Fig. 3

Galaxy Cluster Abell 2390

Hubble Composite Image

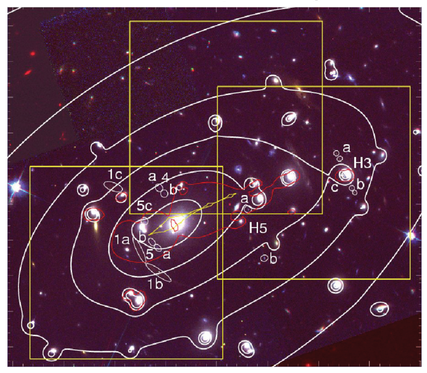

Lensing Derived Mass Map

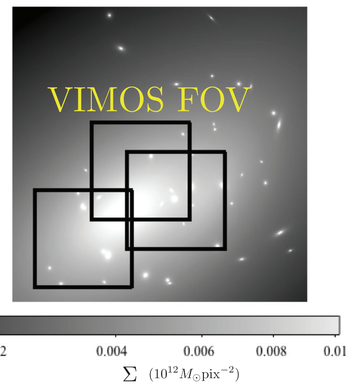

HST WFPC-2 images were obtained for the galaxy clusters Abell 2667 (A2667) and 2390 (A2390), at $z_{\rm cl} = 0.233$ and 0.228. For A2667, the filters F450W, F606W, and F814W were used. For A2390, F555W and F814W were used. ISAAC images were used to measure J-H colors for A2667; HST images were used to determine I-V colors for A2390. Using techniques described in Covone et al. (2005), a multi-component lensing model was fit to the locations of strong lensing arcs/arclets; these models were used to generate projected surface density maps for each cluster; the mass map for A2390 is shown in Fig. 3.

The VIMOS IFU has 6400 fibers, and each pointing covers a sky area of $\sim 1' \times 1'$. To resolve the line of interest, we used the LR-Blue grism. The usable range of wavelengths for VIMOS is 4000Å $-$ 6800Å, yielding an axion mass range of $4.5 - 7.7$eV. Data cubes were 'flat-fielded' using continuum arc lamp exposures. The total exposure time for each cluster was 1.08×10^4 s. A2390 was targeted in three pointings; A2667 was targeted in one. The data were reduced using VIPGI and our own routines. Cosmic rays were removed using an automated σ-clipping algorithm; we checked that the removed pixels exhibited the distinct spatial gradients of cosmic rays, in order to make sure that we would not inadvertently remove an axion signal. If axions exist in this mass window, at a rest-frame wavelength $\lambda_{\rm a}$, we would observe a spatially extended emission line whose intensity traces the projected dark-matter density. Because we seek a faint signal near the sky background in intensity, we implement a customized sky-subtraction to optimally extract emission from decaying axions.

We model the data as the sum of a homogeneous sky component and a density-dependent signal, that is $I_{\lambda,i}^{\rm mod} = \langle I_\lambda/\Sigma_{12}\rangle\Sigma_{12,i} + b_\lambda$. The real sky signal may not be homogeneous, but this is maximally conservative. We estimate a 'noise cube' that includes Poisson counting noise, CCD read noise, bias, dark-current, and estimates of the uncertainty in fiber efficiency. We then determine the best fit value of $\langle I_\lambda/\Sigma_{12}\rangle$ at each λ, thus obtaining 1D spectra, as shown for A2390 in Fig. 4. No evidence for axion decay emission was seen in either cluster. The sky subtraction procedure is repeated using best-fit NFW/King density profiles,and the profile that sets the least conservative limit on $\langle I_\lambda/\Sigma_{12}\rangle$ at each λ is used.

The quality of sky background subtraction may vary as a result of spatial and temporal variations in the sky background from night to night. If it is not due to axion decay, the density correlated emission might also genuinely vary between clusters. The quantity $\langle I_\lambda/\Sigma_{12}\rangle$, however, will by definition be independent of these factors. A simple error weighted mean of the upper limits obtained from the two clusters would thus erroneously increase the upper limit placed on ξ. If two clusters yield different best-fit values for $\langle I_\lambda/\Sigma_{12}\rangle$, $\langle I_\lambda/\Sigma_{12}\rangle$ must be bounded from above by the lesser of these two. We also searched for a line using cross-correlation techniques, and obtained similar limits.

V. Results

Fig. 4

Reduced one-dimensional spectrum with $\xi = 0.03$ axion lines superimposed

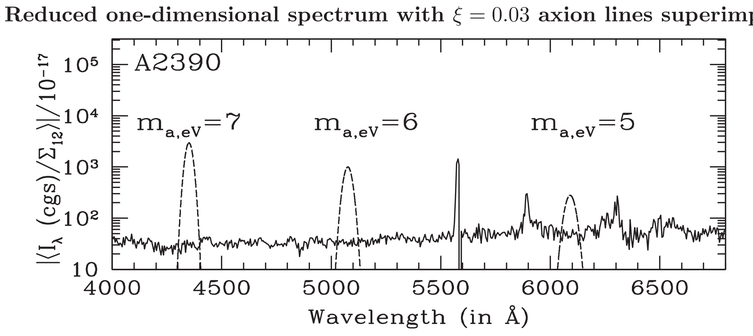

New limits to two-photon coupling of the axion

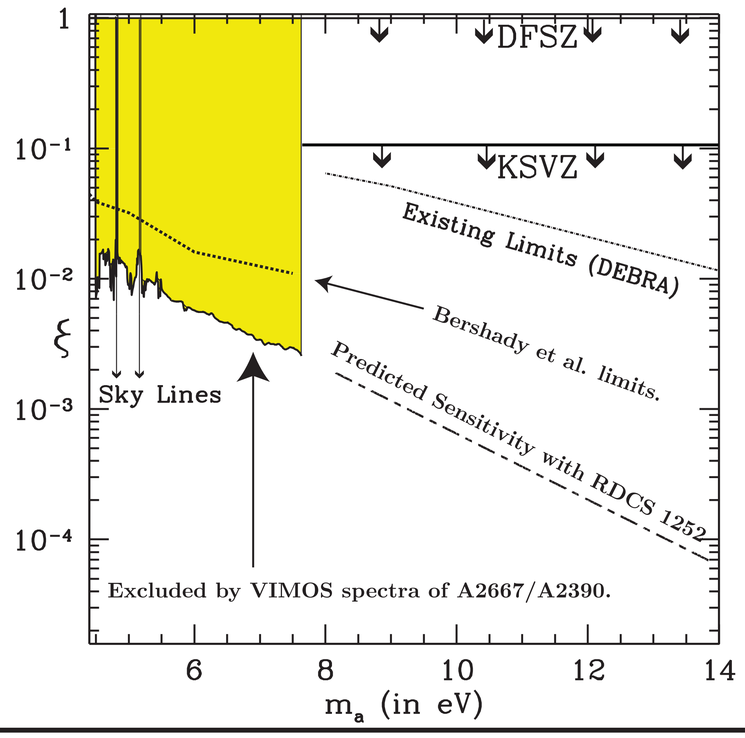

VI. Discussion

The limits to ξ we obtained are compared with past work in Fig. 4, and are a factor of ~ 3 tighter. This level of improvement is to be expected given the greater exposure, the null signal, and the scaling of intensity with ξ. The tightest limits came from A2390. We also re-analyzed the flux limits of Bershady et al., using modern best-fit mass profiles for the clusters A2218, A2256, and 1413, and present-day best fit values for cosmological parameters. Depending on $m_{\rm a}$, we improve on their rescaled limits by a factor of $2.1 - 7.1$. Our limits to ξ are independent of any assumptions about the dynamics of the cluster, and thus robust, ruling out DFSZ and KSVZ axions in the mass window probed, unless the theoretical prediction for ξ is suppressed.

In Fig. 4, we also determine our future sensitivity to axions in the mass window $14 - 20$ eV, assuming similar quality IFU spectra for the high-redshift lensing cluster RDCS 1252 ($z \approx 1.24$), and similar cluster mass profiles. The sensitivity actually improves with redshift, due to the scaling of intensity with axion mass. Weak and strong-lensing maps already exist for RDCS1252, though we hope to augment these with our own after we obtain VIMOS spectra of the cluster.

In the past few years, high-precision CMB and large-scale-structure (LSS) measurements have become available and allowed new constraints to axion parameters in this mass range. In particular, axions in the few-eV mass range behave like hot dark matter and suppress small-scale structure in a manner much like neutrinos of comparable masses. Hannestad et al. (2005) shows that such arguments lead to an axion-mass bound $m_{\rm a} \leq 1.05$ eV. Still, given uncertainties and model dependences, it is important in cosmology to have several techniques as verification. For example, in extended, low-temperature ($\sim$ MeV) reheating models, light relics like axions and neutrinos are produced non-thermally and have suppressed abundances, evading CMB/LSS bounds, but may still show up in telescope searches for axion decay lines. Finally, other dark-matter candidates may show up in such searches; the sterile neutrino is one example.

VII. Simulations

Previous cluster searches for axions used long-slit spectroscopy. Our use of IFU data is novel, so to check that details of IFU data analysis were not thwarting our search, we conducted a simulation at 10 candidate axion masses spanning our full probed range, using $3 - 4$ values of ξ for each mass. The first value was chosen to be slightly below $(5 - 10\%)$ the limit on ξ set by preceding techniques, while the second was chosen to be slightly above the upper limit. The third and fourth values were chosen to be in considerable (factors of 2 and 10, respectively) excess of the upper limit. For all simulated axion masses, visual inspection of the data cube yields clear evidence for the inserted line when ξ exceeds the imposed upper limit. An example is shown in Fig. 5. We then applied the same routine used to extract upper limits to ξ to recover the simulated ξ value. When the simulated value of ξ exceeded the upper limit, we recovered the correct value in all cases to a precision of $5 - 10\%$.

Fig. 5

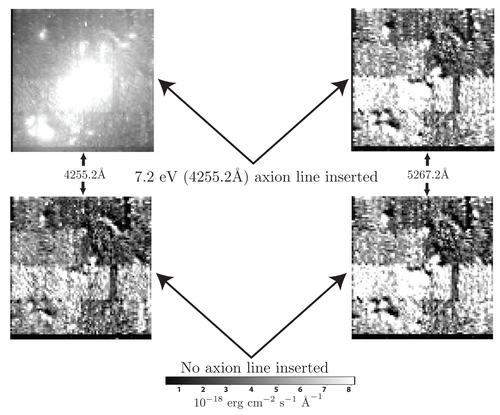

VIII. Sterile Neutrinos

Our data also constrain the decay rate of other ~ 5 eV relics, such as sterile neutrinos. Although the prevailing paradigm places the sterile-neutrino mass in the keV range, some experimental data can be fit by introducing a hierarchy of sterile neutrinos, at least one of which is in the $1 - 10$ eV range and could oscillate to produce photons in our observation window. Our flux limits impose the constraint $B \leq 10^{-5}$, where B is a factor encoding the effects of early-universe production and present day decay of sterile neutrinos. In conventional models, $B = \sin^4(2\theta)/10^{11}$. The parameter B encodes the effects of both the early-universe production and the decay of sterile neutrinos. By definition, $B \leq 10^{-11}$, and so optical data only constrain sterile neutrinos if some novel mechanism increases the oscillation rate by many orders of magnitude.

References

M. A. Bershady, M. T. Ressell, and M. S. Turner, Phys. Rev. Lett. **66**, 1398 (1991).

R. D. Peccei and H. R. Quinn, Phys. Rev. Lett. **38**, 1440 (1977).

M. S. Turner, Phys. Rev. Lett. **60**, 1101 (1988).

T. Moroi and H. Murayama, Phys. Lett. **B440**, 69 (1998), hep-ph/9804291.

G. Covone, J.-P. Kneib, G. Soucail, J. Richard, E. Jullo, and H. Ebeling, Astron. Astrophys. **456**, 409 (2006), astro-ph/0511332.

T. W. Kephart and T. J. Weiler, Phys. Rev. Lett. **58**,171 (1987).

S. Hannestad, A. Mirizzi, and G. Raffelt, JCAP **0507**, 002 (2005), hep-ph/0504059.

Acknowledgements

The authors thank Ted Ressell and Matthew Bershady for helpful discussions. D.G. was supported by a Gordon and Betty Moore Fellowship. G.C. acknowledges support from the European Community via the Marie Curie European Re-Integration Grant n.029159. J-P.K. acknowledges support from the CNRS. M.K. was supported in part by DoE DE-FG03-92-ER40701, NASA NNG05GF69G, and the Gordon and Betty Moore Foundation. A.W.B thanks the Alfred P. Sloan Foundation and Research Corporation for support. E.J. is supported by a PhD fellowship from ESO. Based on observations made with ESO Telescopes at the Paranal Observatories (program ID 71.A-3010), and on observations made with the NASA/ESA Hubble Space Telescope, obtained from the data archive at the Space Telescope Institute STScI is operated by the association of Universities for Research in Astronomy, Inc. under the NASA contract NAS5-26555.